



## OPEN ACCESS

## EDITED BY

Mingjie Liu,  
Southwest Petroleum University, China

## REVIEWED BY

Cunhui Fan,  
Southwest Petroleum University, China  
Yongmei Zhang,  
China University of Geosciences, China

## \*CORRESPONDENCE

Meiyan Fu,  
✉ fumeiyan08@cdut.cn

RECEIVED 08 March 2023

ACCEPTED 26 May 2023

PUBLISHED 16 June 2023

## CITATION

Dong S, Fu M, Song R, Guo H and Shen Q (2023), Diagenesis and reservoir quality of Neoproterozoic dolomitized microbialites following multi-stage diagenetic fluid activity: a case study of the Sinian Dengying Formation, China. *Front. Earth Sci.* 11:1181863. doi: 10.3389/feart.2023.1181863

## COPYRIGHT

© 2023 Dong, Fu, Song, Guo and Shen. This is an open-access article distributed under the terms of the [Creative Commons Attribution License \(CC BY\)](https://creativecommons.org/licenses/by/4.0/). The use, distribution or reproduction in other forums is permitted, provided the original author(s) and the copyright owner(s) are credited and that the original publication in this journal is cited, in accordance with accepted academic practice. No use, distribution or reproduction is permitted which does not comply with these terms.

# Diagenesis and reservoir quality of Neoproterozoic dolomitized microbialites following multi-stage diagenetic fluid activity: a case study of the Sinian Dengying Formation, China

Shuyi Dong<sup>1,2</sup>, Meiyan Fu<sup>1,3\*</sup>, Rongcai Song<sup>1,3</sup>, Hengwei Guo<sup>3</sup> and Qiuyuan Shen<sup>4</sup>

<sup>1</sup>State Key Laboratory of Oil and Gas Reservoir Geology and Exploitation, Chengdu University of Technology, Chengdu, China, <sup>2</sup>College of Earth Science, Chengdu University of Technology, Chengdu, China, <sup>3</sup>College of Energy, Chengdu University of Technology, Chengdu, China, <sup>4</sup>Shunan Gas Production Plant, PetroChina Southwest Oil and Gasfield Company, Luzhou, China

Neoproterozoic marine microbialites have been targets for exploration and hydrocarbon reservoir development. The original depositional fabric and diagenesis control the pore systems of microbialites, leading to the complicated origin of microbialite reservoirs. This study aimed to reveal the origin of microbialite reservoirs following multi-stage diagenetic fluid activity in the fourth Member of the Dengying Formation in the central Sichuan Basin in southwestern China. The fourth Member of the Sinian Dengying Formation developed dolomitized microbialites, mainly including stromatolites, laminates, and thrombolites. Based on the background of tectonic movement, petrology and geochemistry examinations were executed to analyze the origin of the microbialite reservoir. Based on the cathodoluminescence and the homogenization temperature of the brine inclusions, it is credible that there were four stages of diagenetic fluid activities in the burial diagenesis. In the first stage, the microbialite reservoir was charged by oil in the Silurian period, with evidence from residual asphalt around the pores. In the second stage, dolomite precipitated to incompletely fill the pore spaces. In the third stage, the silica-rich diagenetic fluid with high temperature resulted in the precipitation of authigenic quartz. In the last stage, the oil charged again during the Triassic period, followed by siliceous filling, with residual asphalt filling the pore spaces. There were two stages of subaerial emergence, which occurred in two episodes of the Sinian-Early Cambrian Tongwan movement. The evidence for the two tectonic events includes two phases of dolomites with meteoric water origin, two cycles of V, Sr, and Na element profiles, two instances of negative excursion  $\delta^{18}\text{O}$  isotope, and two cavity layers. By comparison, the karstification of reservoirs in the Tongwan III episode could generate a higher quality of reservoir than that in the Tongwan II episode. As a result, the quality of the microbialite reservoir from the fourth Member of the Dengying Formation was mainly improved by the subaerial exposure in the Tongwan III episode and then was partly destroyed by the siliceous filling. The identification of multi-staged diagenetic fluid charging can illustrate the evolution of the reservoir quality of Neoproterozoic microbialites.

## KEYWORDS

Sichuan Basin, member 4 of Dengying Formation, microbial carbonate reservoir, Tongwan movement, reservoir quality

## 1 Introduction

Microbialites are the product of microbial activity; e.g., the precipitation of carbonate minerals induced by benthic microbial community or its capture and binding of carbonate particles (Riding, 2000), mainly including stromatolite, thrombolite, dendrolite, leiolite, and laminate (Burne, 1987; Terra et al., 2010; Mancini et al., 2013; Bahniuk et al., 2015). Generally, in terms of sedimentary structure, microbialite rocks can be identified as columnar, dome, mound, clotted, and slow wave structures on a macro scale (Shapiro, 2000; Chen et al., 2014; Tang et al., 2017). On a microscale, there are spherical, ellipsoid, and rod structures, as well as filaments and extracellular polymers in microbialite rocks (Shapiro, 2000; Dupraz et al., 2004; Bahniuk et al., 2015; Catto et al., 2016). The void spaces of microbialite rocks can be identified as window-like pores, framework pores, intergranular pores, etc. (Woo et al., 2010; Chafetz, 2013; Hao et al., 2018). Generally, the original depositional fabric and diagenesis are important controlling factors for the pore systems of microbialite reservoirs (Bosence et al., 2015). High permeabilities are associated with vuggy microbial facies (thrombolites) and tight intervals with non-microbial facies (Amthor, 2013). During early to late diagenesis, dissolution and fracturing increase porosity and permeability, and cementation and pressure solutions may reduce pore space (Roehl and Choquette, 1985). The old and deeply buried Neoproterozoic microbial dolostone reservoirs will have more complicated origins following multi-stage fluid activity during burial diagenesis. However, the quality responses of microbialite reservoirs to multi-stage water-rock reactions are obscure.

The microbialite reservoir of the Sinian Dengying Formation in China has attracted attention for its extensive natural gas resources (Luo et al., 2015; Liang et al., 2019; Zhang et al., 2020). With the natural gas exploration of the Sinian Dengying Formation, many studies have emphasized the karstification control of the reservoir quality rather than sedimentary facies. The reservoir spaces inherited from sedimentary structures rearranged during diagenesis. The dissolved pores are the main reservoir spaces of microbialite rocks from the fourth Member of the Sinian Dengying Formation, including non-fabric selective dissolved pores, vugs, and cavities. It has been suggested that the quality of microbialite reservoirs from the Sinian Dengying Formation has little correlation with sedimentary structure, while the dissolution might be a key factor for the reservoir quality of these carbonate rocks (c.f. Davies et al., 2006; Gale et al., 2007; Chen, 2010; Wang et al., 2014). Leaching of meteoric water during the penecontemporaneous diagenetic period (Xu et al., 2022) and regional exposure karstification during the long subaerial diagenetic period (Xia et al., 2022; Yan et al., 2022; Gu et al., 2023) were the origins of the reservoir in the Sinian Dengying Formation. However, the sedimentary structure of microbialite rocks could influence the distribution of the dissolved pores.

Previous studies have shown that the Sinian Dengying Formation has experienced multiple episodes of tectonic movements; e.g., the successive Sinian-Early Cambrian Tongwan

movement, Caledonian movement, Indosinian movement, and Yanshan movement (Liang et al., 2014). Among them, the Tongwan movement resulted in the subaerial emergence of the Dengying Formation to create the subaerial karstification. However, the episodes of the Tongwan movement remain controversial. There is disagreement regarding whether two or three episodes of Tongwan movement occurred (Wang et al., 2014; Yang et al., 2014; Hao et al., 2017). As a result, the timing of the karstification of the Dengying Formation is debated. Furthermore, multiple stages of diagenetic fluid activity occurred in the Dengying Formation during burial diagenesis (Liang et al., 2014). Due to the uncertainty of the timing of the karstification and multiple stages of fluid activity in the Dengying Formation, the effects of sedimentation, eodiagenesis, and telodiagenesis on the quality of the microbialite reservoir are controversial (e.g., Zhu et al., 2020).

In the present study, data from drilling cores and logging wells, core observations, identification of thin sections, and geochemical measurement were used to analyze the diagenetic process and paragenesis of the microbialite from the fourth Member of Dengying Formation in the Gaoshiti area of Sichuan Basin, China. The timing of karstification and the stages of fluid activity were reconstructed to establish the pore evolution of microbialite reservoirs.

## 2 Geological setting

The Gaoshiti area is located at the eastern of the paleo-uplift of the central Sichuan Basin, China (Figure 1). The marine carbonate rocks developed in the Sinian-Middle Triassic period in the study area (Liao et al., 1999; Wei et al., 2015; Fan et al., 2022). During the Sinian period, the South China Plate featured a warm and hot climate, with a temperature between 20°C and 30°C (Bengtson and Zhao, 1992; Grotzinger et al., 2000; Narbonne, 2005). During the sedimentary period of the Dengying Formation, the Gaoshiti area in the Sichuan Basin was on the margin of the intra-shelf depression (Wei et al., 2015; Jin et al., 2017; Mo, 2017). During the deposition of the Upper Sinian Dengying Formation in Sichuan Basin, the paleoclimate was arid and hot (Zhang et al., 2004). The carbonate platforms deposited during the Dengying age mainly included microbial mounds, intraclastic shoals, platform flats, and lagoons (Yan et al., 2022). During this period, homonemae and stromatolites (e.g., cyanobacteria) were widespread. According to lithology and paleontological characteristics, the Dengying Formation was divided into four members from bottom to top. Among them, the first Member of the Dengying Formation (D1) was mainly composed of light gray-dark gray dolomicrite. The second Member (D2) was mainly composed of light gray dolostones containing algae, with a stratabound, agglomerate, and grape-like structure. The lithologies of the third Member were mainly dark gray and blue-gray mudstone, sandy dolomicrite, and dolomitic sandstone. The fourth Member (D4) was composed of microbial dolostones, mainly including light gray-dark gray stratabound very

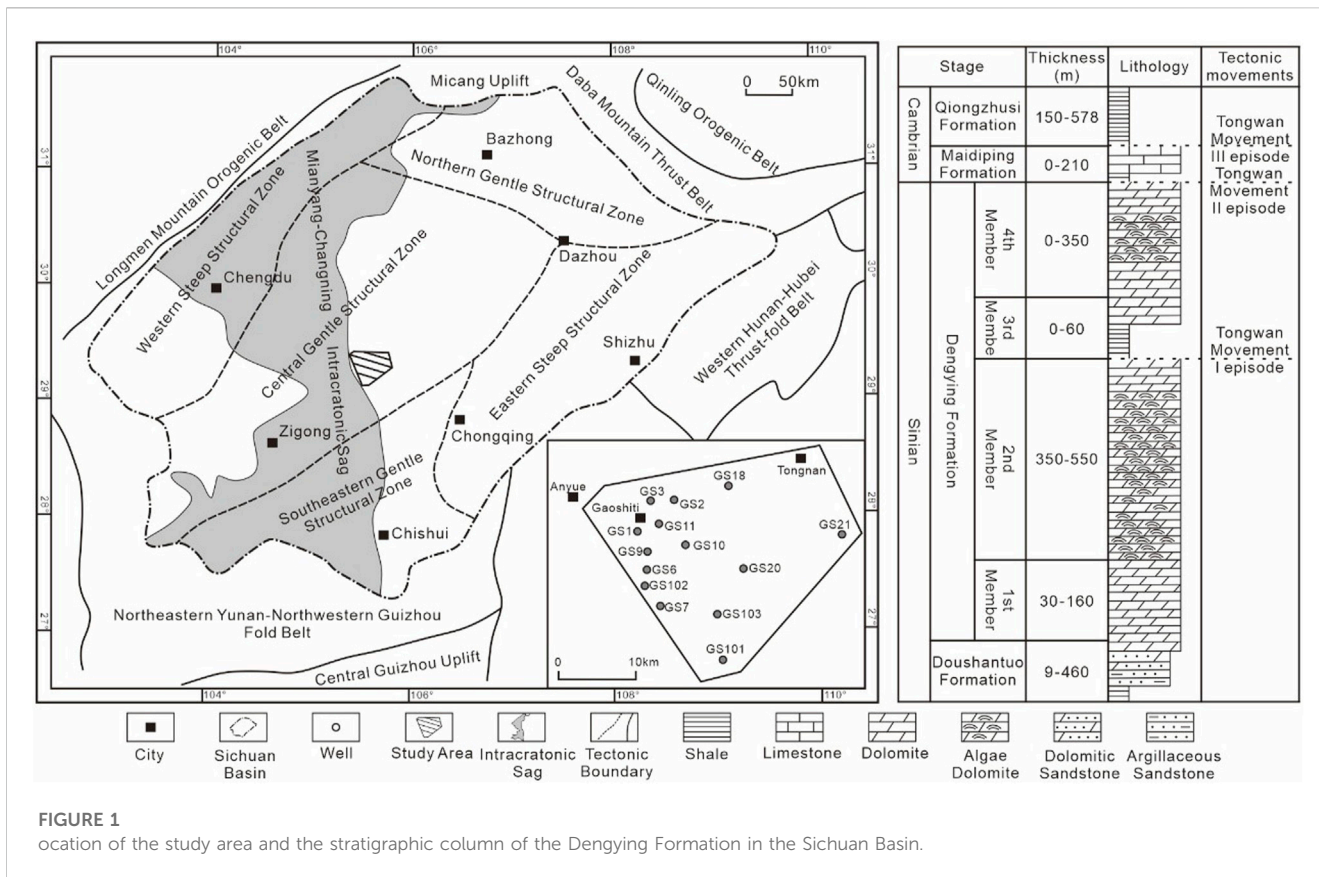


**FIGURE 1** Location of the study area and the stratigraphic column of the Dengying Formation in the Sichuan Basin.

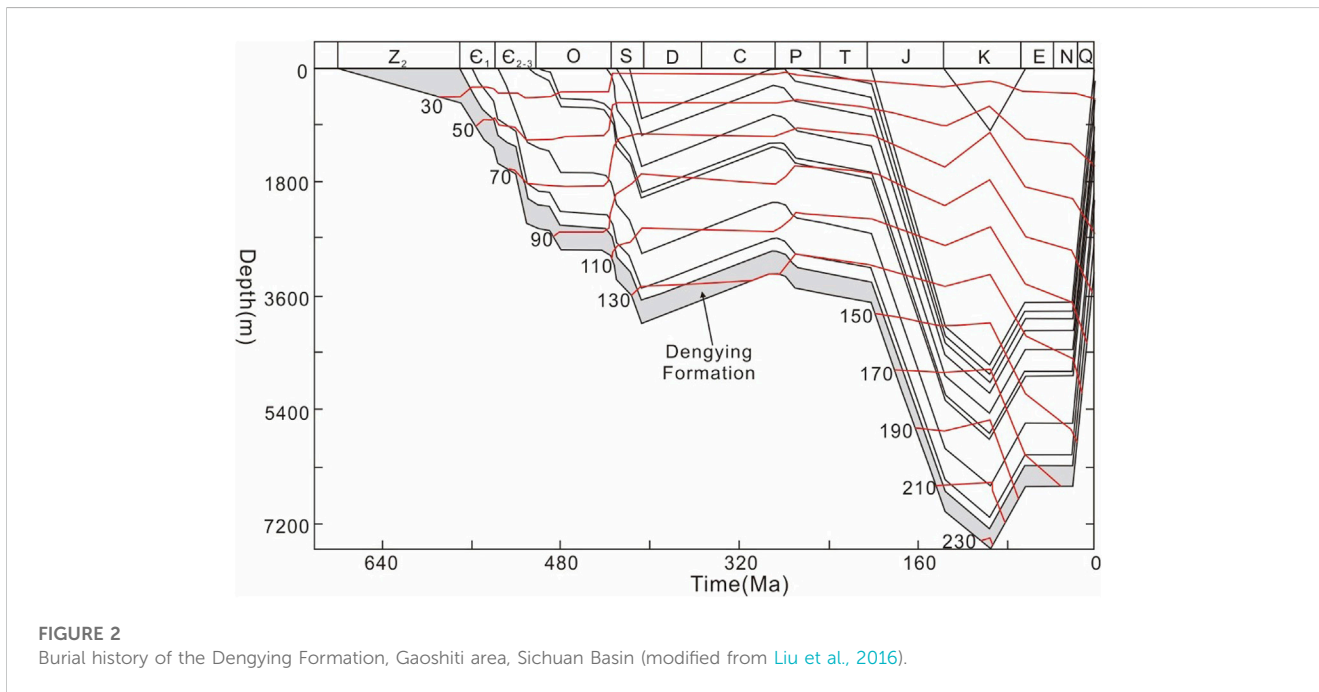


**FIGURE 2** Burial history of the Dengying Formation, Gaoshiti area, Sichuan Basin (modified from Liu et al., 2016).

fine crystalline dolostone, doloarenite, and algal-rich dolostone, partially bedded with siliceous strips and chert concretions.

The Tongwan movement occurred during the deposition of the Late Sinian Dengying Formation to the Early Cambrian Maidiping Formation (Hao et al., 2017; Mo, 2017). Three episodes of Tongwan

movement with uplifting have been suggested (Wang et al., 2014), with durations of about 20 Ma (Huang et al., 1974; Yang et al., 2014c). Episode I of the Tongwan movement resulted in the formation of unconformity between Members 2 and 3 of the Dengying Formation. Episode II of the Tongwan movement led

**TABLE 1** Sampling information on Member 4 of the Dengying Formation in the Gaoshiti area, Sichuan Basin.

No.	Depth/m	Major element	Trace element	C, O isotopes	Sr isotope	Homogenization temperature of the inclusion
GS1-1	4956.00					√
GS1-3	4957.00	√	√	√		√
GS1-4	4960.00	√	√			√
GS1-5	4970.28	√	√	√		√
GS1-6	4975.00	√	√	√	√	√
GS1-8	4977.00	√	√	√	√	√
GS1-9	4978.00	√	√	√		√
GS1-10	4979.00	√	√	√	√	√
GS1-11	4980.00	√	√	√	√	√
GS1-12	4980.00	√	√	√		√
GS1-14	4981.00	√	√	√		√
GS1-15	4986.00	√	√	√		√
GS1-16	4960.00	√	√			√
GS1-17	4966.89	√	√			√
GS7-10	5294.02	√	√	√	√	√
GS7-11	5301.48	√	√	√		√
GS7-13	5306.35	√	√	√		√
GS7-16	5324.80	√	√	√		√
GS7-20	5345.26	√	√	√	√	√
GS7-22	5265.28	√	√	√		√

to the occurrence of unconformity between Member 4 of the Dengying Formation and the Cambrian Maidiping Formation. Episode III of the Tongwan movement finally caused the formation of unconformity between the Cambrian Maidiping Formation and the Cambrian Qiongzhusi Formation. In the Gaoshiti-Moxi and Ziyang areas, Tongwan episodes II and III overlapped (Luo et al., 2018), resulting in the complete erosion of the Maidiping Formation. The study area was subsidence in the Late Neoproterozoic Silurian. Furthermore, during the Hercynian movement, there was a large-scale uplift of the strata in the study area. Then, the study area was continuous subsidence, with a maximal extent in the Jurassic period. In the last stage, the study area was uplifted in the Yanshan and Himalayan movement (Figure 2) (Hartnady, 1986; Tong, 1992; Piper, 2000; Wei et al., 2015). In the Gaoshiti area, as a result of the Tongwan movement,

the fourth Member of the Dengying Formation experienced erosion caused by karstification (Hao et al., 2017). Due to the erosion in the Tongwan period, the residual thickness of D4 ranges from 0 to 350 m in the Gaoshiti area, with the largest thicknesses in the wells GS1 and GS3.

### 3 Samples and methods

In this study, cores from five drilling wells were collected from PetroChina Southwest Oil and Gas Field Company, China (Table 1). A total of 78 thin sections were identified for lithology, mineralogy, and diagenetic alterations. A total of 24 thin sections were observed under cathode luminescence (CL) using a CITL/CL8200 MK5-2 (made in England) cold cathode instrument. The voltage was 14 kV,

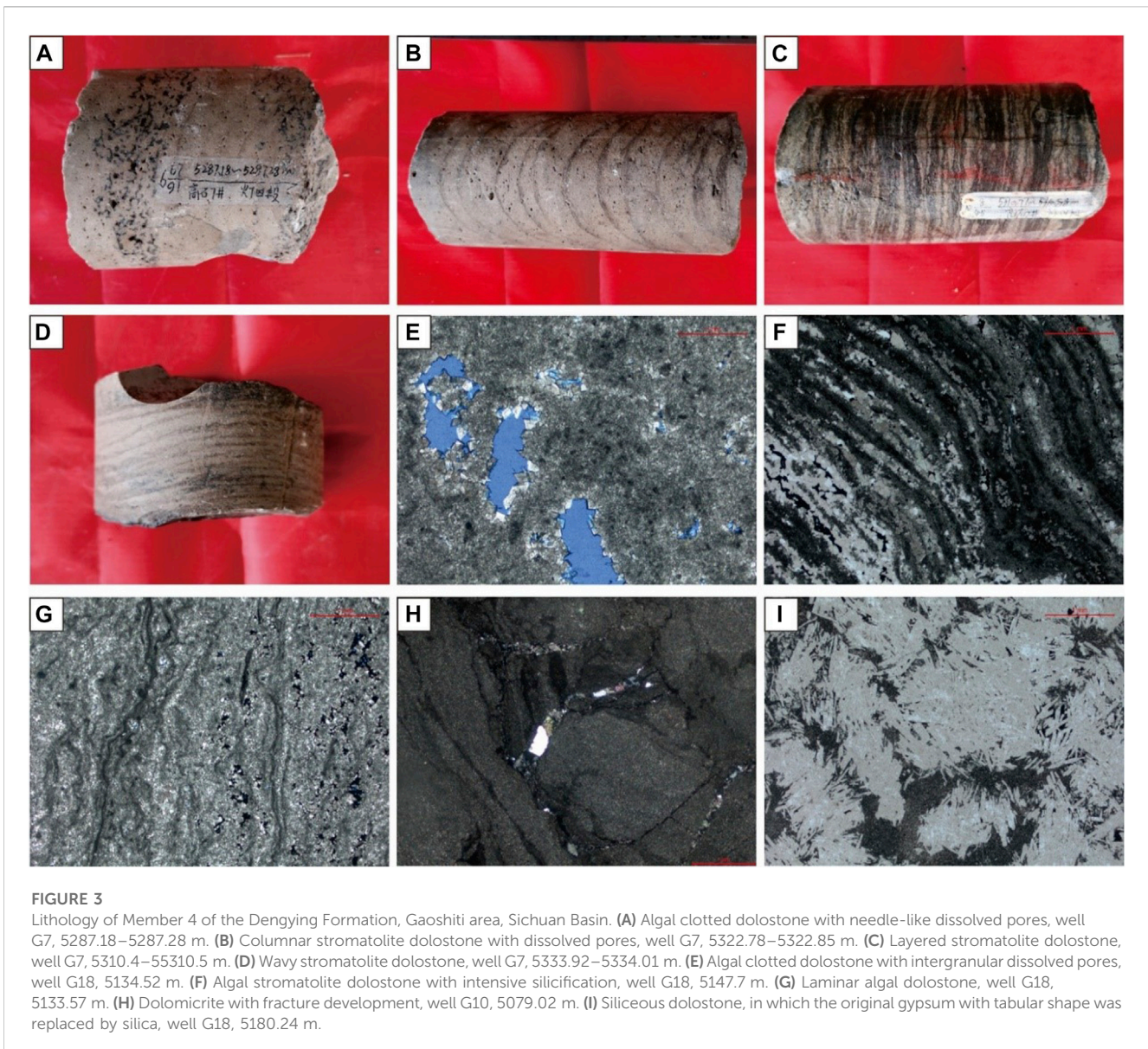


**FIGURE 3**

Lithology of Member 4 of the Dengying Formation, Gaoshiti area, Sichuan Basin. (A) Algal clotted dolostone with needle-like dissolved pores, well G7, 5287.18–5287.28 m. (B) Columnar stromatolite dolostone with dissolved pores, well G7, 5322.78–5322.85 m. (C) Layered stromatolite dolostone, well G7, 5310.4–53310.5 m. (D) Wavy stromatolite dolostone, well G7, 5333.92–5334.01 m. (E) Algal clotted dolostone with intergranular dissolved pores, well G18, 5134.52 m. (F) Algal stromatolite dolostone with intensive silicification, well G18, 5147.7 m. (G) Laminar algal dolostone, well G18, 5133.57 m. (H) Dolomitic dolostone with fracture development, well G10, 5079.02 m. (I) Siliceous dolostone, in which the original gypsum with tabular shape was replaced by silica, well G18, 5180.24 m.

and the current was 380  $\mu$ A. The CL images were captured with 20-s exposure times.

A THMS600 Cooling-Heating Stage (Linkam Scientific, Surrey, England) was used to measure the homogenization temperature of the fluid inclusions enclosed in the quartz and dolomite cement in dolostones. The temperature range of the instrument is from  $-196^{\circ}$  to  $600^{\circ}$ C with a precision of  $<0.1^{\circ}$ C. The rate of temperature increase can be controlled to within  $1^{\circ}$ C/min when approaching the critical point.

The element compositions of the carbonate rocks were detected using an inductively coupled plasma atomic emission spectroscopy (ICP-AES) (Optima 5300 V, PerkinElmer Company) and inductively coupled plasma mass spectrometry (ICP-MS). The major elements were detected by ICP-AES and ICP-MS, respectively.

Sixteen core samples of dolostones from wells GS1 and GS7 were measured for their bulk carbonate carbon and oxygen stable isotope

values on a MAT253 stable isotope ratio mass spectrometer (Thermo Scientific, Waltham, MA, United States). All the isotope data were calculated as the per-mil deviation from the Pee Dee Belemnite (PDB) standard. Samples were processed using the phosphoric acid method.

Sr isotopes of seven dolostones from wells GS1 and GS7 were measured by Triton plus thermoionization mass spectrometry (Thermo Fisher Scientific, Germany). The error of NBS987 is  $<0.002\%$ .

## 4 Results

### 4.1 Petrographic features

According to core observation and thin section identification, the lithologies of the D4 member are mainly algal-rich dolostones;

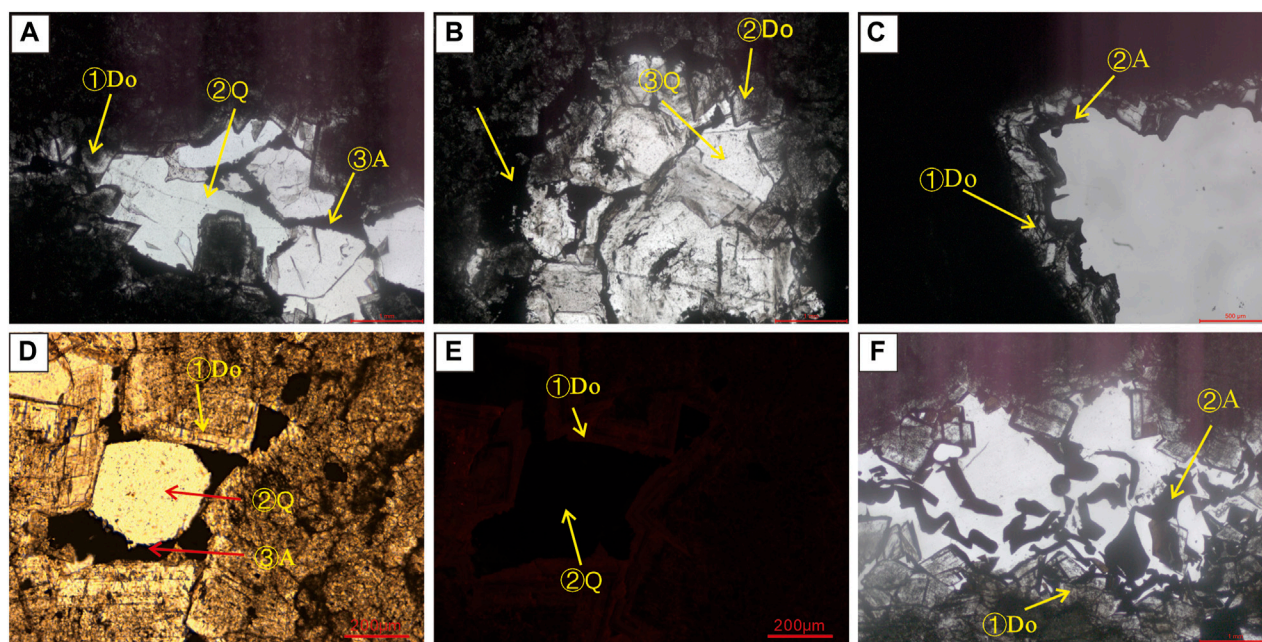


**FIGURE 4**

illing sequences of dolostones from Member 4 of the Dengying Formation, Gaoshiti area, Sichuan Basin. (A) Dolomite, quartz, and asphalt filled with dissolved pores, well G1, 4957.00 m. (B) Dolomite, quartz, and asphalt filled with dissolved pores, well G1, 4957.00 m. (C) Dolomite and asphalt filled within the vug, well G10, 5079.73 m. (D) Dolomite and quartz (single polarized light) filled within the vug, well G1, 4957.00 m. (E) Dolomite and quartz filled within the vug (CL), well G1, 4957.00 m. (F) Vug filled with fine to medium dolomite, with a scattered distribution of asphalt, well G1, 4975.00 m.

e.g., stromatolite, thrombolite, and laminate. In addition, there are also algal-poor dolostones; e.g., dolomicrite, granular dolostone, and gypsodolomite (Figure 3).

Thrombolite dolostone is the main type of algal-rich dolostone in the study area. Thrombolite dolostone was mostly distributed in wells GS1 and GS7, as well as in the upper part of the D4 member in well GS18. Needle-like dissolved pores of thrombolite dolostone were observed frequently in the cores (Figure 3A). In addition, intergranular dissolved pores developed, which were incompletely filled with dolomite and asphalt.

Stromatolite dolostone is also important in the study area and is mainly distributing in wells GS7 and GS18. The columnar (Figure 3B) and layered (Figure 3C) stromatolite could be observed in the cores of well GS7. Only wavy stromatolite was observed in the cores from well GS18 (Figure 3D). The stromatolite dolostone in well GS7 had a great number of dissolved pores and cavities (Figure 3E). However, the stromatolite dolostone in well GS18 was highly silicified along the framework of the algal laminated strip, with few pores (Figure 3F).

Laminate dolostone was distributed in the cores from the five drilling wells. Based on the identification of the thin sections, the dark layer of laminate dolostone is sparse, with fine lines. The crystal size of laminar algal dolostones is micritic, with the reservoir space showing bird's eye and window-like pores (Figure 3G).

The dolomicrite is very tight without visible pores. The pore types of dolomicrite are mainly intercrystalline micropores. In addition, there are some micro-fractures (Figure 3H). The horizontal fractures are open and without fillings. The dissolved fractures are fully or incompletely filled with asphalt and dolomite.

Gypsodolomite is observed in well GS18. Generally, gypsum replaced by silica in the burial diagenesis retains the tabular shape of gypsum (Figure 3I). There are almost no visible pores in the gypsodolomite.

## 4.2 Diagenesis and diagenetic minerals

Dolomite, quartz, and asphalt are the main fillings in the dolostones in member D4, with minor calcite. Among them, authigenous dolomite is generally distributed as the lining of the vug (Figure 4A), with relatively euhedral fine crystal morphology. Occasionally, euhedral coarse crystalline dolomites can be seen in large, dissolved cavities. Under cathodoluminescence, the fine crystalline dolomites are generally dark brown-red or red in color, while those of coarse crystalline dolomites are relatively bright. This indicates a high Fe/Mn ratio of the dolomite fillings (Frank, 1982). The shapes of fluid inclusions within the dolomites are regular, mainly elliptical or circular. The homogenization temperatures of the fluid inclusions enclosed in dolomite mainly range from 120°C to 160°C (Figure 5).

Authigenous quartz can be observed in the dissolved pores. The authigenous quartz postdated the precipitation of authigenous dolomites (Figures 4A, B). Under cathodoluminescence, the quartz is generally dull in color (Figures 4D, E). The homogenization temperature of the fluid inclusions within the authigenous quartz is generally above 160°C, mainly distributed from 180°C to 200°C, even up to 260°C (Figure 5).

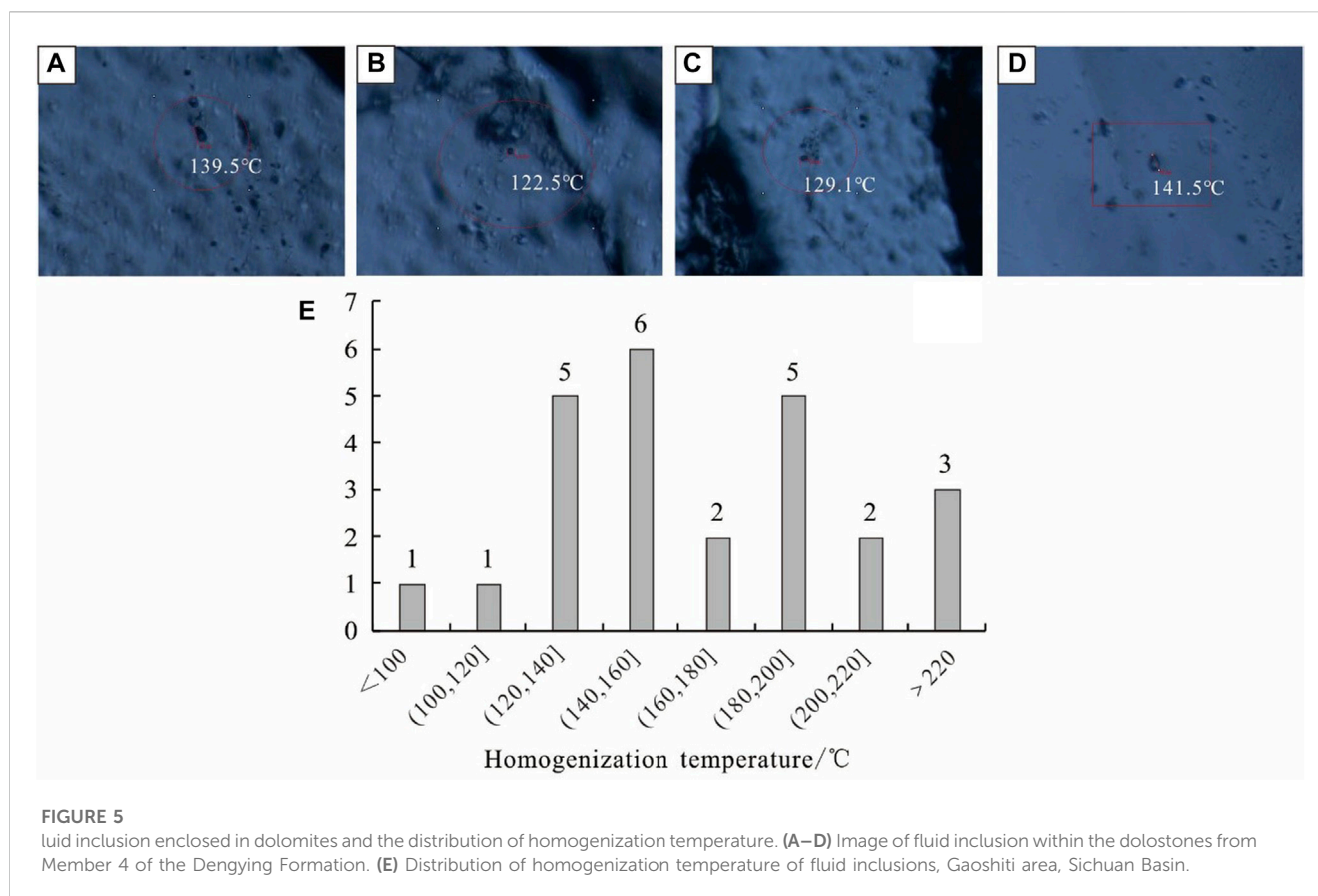


**TABLE 2** Concentrations of major and trace elements of samples from Member 4 of the Dengying Formation, Gaoshiti area, Sichuan Basin.

No.	GS1-3	GS1-4	GS1-5	GS1-6	GS1-8	GS1-9	GS1-10	GS1-11	GS1-12	GS1-14	GS1-15	GS1-16	GS1-17
Depth	4957.00	4960.00	4970.28	4975.00	4977.00	4978.00	4979.00	4980.00	4980.50	4981.00	4986.00	4960.50	4966.89
Al <sub>2</sub> O <sub>3</sub> %	0.665	0.219	0.152	0.064	0.122	0.098	0.054	0.137	0.052	0.152	0.064	0.276	0.234
TFe <sub>2</sub> O <sub>3</sub> %	2.365	0.571	0.255	0.228	0.31	0.399	0.223	0.261	0.331	0.315	0.202	0.634	0.733
Na <sub>2</sub> O%	0.077	0.096	0.038	0.039	0.051	0.055	0.008	0.07	0.05	0.039	0.014	0.07	0.058
Ti	266.345	82.676	47.141	36.14	53.951	34.831	43.588	61.201	30.023	53.434	36.635	114.635	75.646
V	19.24	10.702	5.869	11.879	11.009	6.839	5.987	6.879	6.931	7.061	7.876	19.719	9.69
Mn	1732.586	1199.26	915.62	842.465	682.352	930.748	527.322	297.938	626.824	335.54	541.97	1396.108	813.751
Ni	9.835	3.997	2.575	2.511	2.874	2.397	2.665	3.058	1.553	2.601	2.16	5.885	4.132
Sr	90.509	40.217	47.422	39.44	81.581	65.044	34.231	91.704	71.363	84.623	68.201	46.647	46.793
Ba	174.989	50.445	106.644	750.34	521.943	355.44	236.167	197.802	422.072	274.923	165.073	335.55	207.1

The study area shows a small amount of solid asphalt fill in the pores and cavities of the dolostones (Figures 4C, F). According to the petrographic features, there were three phases of oil-charging related to asphalt formation. The early asphalt formed before the second phase of asphalt formation occurred after the authigenous dolomites (Figures 4A, B). The last phase of asphalt postdated the precipitation of the authigenous quartz.

### 4.3 Major and trace element composition

The major and trace element contents of the algal-bearing dolostones in well GS1 are shown in Table 2. The rare earth element concentrations have been shown in Table 3. Among them, the Al<sub>2</sub>O<sub>3</sub> content is 0.052%–0.665% (average 0.176%). The total Fe<sub>2</sub>O<sub>3</sub> content is 0.223%–2.365%, (average 0.525%). Except for GS1-3, the TFe<sub>2</sub>O<sub>3</sub> content in the samples is <0.8%.

**TABLE 3 Rare earth element concentrations of samples from Member 4 of the Dengying Formation, Gaoshiti area, Sichuan Basin.**

No.	GS1-3	GS1-4	GS1-5	GS1-6	GS1-8	GS1-9	GS1-10	GS1-11	GS1-12	GS1-14	GS1-15	GS1-16	GS1-17
Depth	4957.00	4960.00	4970.28	4975.00	4977.00	4978.00	4979.00	4980.00	4980.50	4981.00	4986.00	4960.50	4966.89
La	7.096	1.068	1.499	1.113	1.035	0.752	1.176	1.337	1.009	1.647	0.889	1.598	1.065
Ce	6.315	1.676	2.42	1.756	2.234	1.16	1.836	1.799	1.63	2.078	1.387	2.295	1.578
Pr	0.648	0.204	0.324	0.237	0.209	0.159	0.212	0.232	0.211	0.249	0.179	0.254	0.17
Nd	2.375	0.87	1.317	0.996	0.914	0.641	0.905	0.869	0.875	0.979	0.694	0.96	0.702
Sm	0.494	0.176	0.258	0.213	0.189	0.127	0.196	0.198	0.18	0.177	0.148	0.183	0.141
Eu	0.123	0.045	0.068	0.139	0.109	0.067	0.065	0.061	0.087	0.08	0.054	0.081	0.052
Tb	0.088	0.031	0.041	0.035	0.026	0.019	0.031	0.033	0.029	0.034	0.024	0.031	0.02
Gd	0.555	0.181	0.27	0.246	0.18	0.126	0.193	0.208	0.205	0.211	0.151	0.187	0.134
Dy	0.527	0.172	0.238	0.199	0.13	0.103	0.168	0.18	0.164	0.176	0.119	0.174	0.11
Ho	0.114	0.047	0.045	0.041	0.031	0.018	0.039	0.036	0.035	0.038	0.024	0.045	0.027
Er	0.329	0.114	0.121	0.103	0.085	0.056	0.115	0.097	0.078	0.107	0.067	0.117	0.07
Tm	0.045	0.013	0.017	0.014	0.01	0.007	0.015	0.013	0.012	0.014	0.009	0.015	0.012
Yb	0.25	0.081	0.106	0.07	0.062	0.04	0.085	0.08	0.057	0.089	0.05	0.106	0.065
Lu	0.043	0.013	0.014	0.014	0.01	0.008	0.012	0.012	0.008	0.013	0.009	0.018	0.009
Y	3.235	1.198	1.691	1.485	0.945	0.74	1.273	1.249	1.207	1.2	0.909	1.208	0.73

**TABLE 4 C, O, and Sr isotopes of samples from Member 4 of the Dengying Formation, Gaoshiti area, Sichuan Basin.**

No.	Depth/m	$\delta^{13}\text{C}_{\text{V-PDB}}(\text{‰})$	$\delta^{18}\text{O}_{\text{V-PDB}}(\text{‰})$	$\delta^{18}\text{O}_{\text{V-SMOW}}(\text{‰})$	$^{87}\text{Sr}/^{86}\text{Sr}$
G1-3	4957.00	-0.1	-11.1	19.4	—
G1-5	4970.28	1.5	-8.3	22.4	—
G1-6	4975.00	0.7	-9.9	20.7	0.7102
G1-8	4977.00	2.0	-7.1	23.6	0.7092
G1-9	4978.00	1.7	-8.8	21.8	—
G1-10	4979.00	1.3	-9.1	21.6	0.7088
G1-11	4980.00	1.4	-10.4	20.2	0.7080
G1-12	4980.50	2.8	-4.4	26.4	—
G1-14	4981.00	2.9	-3.3	27.5	—
G1-15	4986.00	2.2	-6.2	24.5	—
G7-10	5294.02	2.8	-8.2	22.5	0.7097
G7-11	5301.48	2.8	-7.8	22.9	—
G7-13	5306.35	1.6	-9.2	21.4	—
G7-16	5324.80	2.0	-8.5	22.2	—
G7-20	5345.26	1.7	-8.9	21.8	0.7094
G7-22	5265.28	3.0	-7.4	23.3	—

The  $\text{Na}_2\text{O}$  content is 0.014%–0.096%. The Mn content is 297.938–1732.586  $\mu\text{g/g}$  (average 834.037  $\mu\text{g/g}$ ). The Sr content ranged from 34.231  $\mu\text{g/g}$  to 91.704  $\mu\text{g/g}$  (average 62.137  $\mu\text{g/g}$ ). The contents of Fe, Ti, Mn, V, Ni, and Sr in the samples (depth

from 4957.0m to 4960.5 m) near the top of the Dengying Formation were significantly higher than those in the samples with burial depths of more than 4960.5 m. However, there is an increasing trend in the middle of the profile near 4975 m. This

implies the potential presence of two important geological surfaces in the vertical section of Member 4 of the Dengying Formation.

## 4.4 Isotope ratios

As shown in Table 4, the composition of the strontium isotope shows an  $^{87}\text{Sr}/^{86}\text{Sr}$  value of the algal-bearing dolostones between 0.70876493 and 0.71018234 (average 0.709202798), slightly higher than the Sr isotope ratio (0.7085) of the contemporaneous seawater in the Late Sinian period (Yang et al., 1999).

The  $\delta^{13}\text{C}$  value of the algal-bearing dolostone ranges from -0.1‰ to 2.8‰ (average 1.9‰). The  $\delta^{18}\text{O}$  value ranges from -11.1‰ to -3.3‰ (average -8.0‰). The average  $\delta^{13}\text{C}$  value of the dolostones in well GS1 (1.6‰) is relatively lower than that in well GS7 (2.3‰). There is a small difference in the  $\delta^{18}\text{O}$  values of the dolostone between wells GS1 and GS7 (average values -7.9‰ and -8.3‰, respectively).

## 5 Discussion

### 5.1 Stages of diagenetic fluid charging

As shown previously, the main fillings in the area are dolomite, quartz, and asphalt. There are different occurrences of fillings. The early dolomite generally grows around the edges of pores and fractures, with euhedral crystals (Figures 4A–C, F). This indicates that when the early dolomite precipitated, there was enough space for the precipitation of authigenous minerals. In the study area, authigenous quartz almost occurred following the precipitation of dolomite and filled the residual space after dolomite filling. Therefore, authigenous quartz mostly appears as anhedral and heteromorphic crystals. The distribution of quartz is obviously controlled by the occurrence of dolomite. The coarser quartz crystals are always associated with fine dolomite crystals (Figure 4B). Conversely, when dolomite grows toward the center of the pores, authigenous quartz is rare or absent (Figures 4A, D). This implies that the precipitation of quartz postdates the early dolomite filling. Meanwhile, under cathodoluminescence, dolomite is generally red or dark red in color (Figures 4D, E). This shows that the precipitation of dolomite occurred at burial diagenesis, with high Fe/Mn ratios (Table 2). Asphalt filling is particularly common in Member 4 of the Dengying Formation in the Gaoshiti area, distributed in most of the dissolved pores and fractures (Figures 4D, F). In most cases, it generally filled the residual space among dolomite or quartz (Figures 4A, C, D, F), implying that the crude oil was charged after the precipitation of dolomite and quartz, and was converted into asphalt due to oil cracking. However, another phase of asphalt fill close to the fracture wall was also observed, which separates the dolomite and the matrix dolomite (Figure 4B). This means that early asphalt predated the precipitation of early dolomite. In brief, the first period of crude oil charging predated the early dolomite, while the second period should postdate the precipitation of dolomite and quartz.

Based on the results of the detailed petrographic observation and fluid inclusion micro-thermometry, the paragenesis of dolostones after deposition has been established (Figure 6). There should be at least four stages of diagenetic fluid charging. The first stage was mainly characterized by crude oil charging. After subaerial emergence, the early crude oil might be oxidized, with residual asphalt. The second stage was characterized by brine, as proven by the precipitation of dolomite. In the third stage, acid or hydrothermal fluids charged into the dolostone reservoir. A large amount of quartz precipitated in this stage, as well as some saddle dolomites of hydrothermal origin. The evidence for the hydrothermal fluid includes the relatively heavy  $^{87}\text{Sr}/^{86}\text{Sr}$  and light  $\delta^{18}\text{O}$  values. Meanwhile, as shown in the standardization of rare earth elements for chondrites, there is a positive anomaly of Eu (Figure 7), indicating hydrothermal fluid charging related to magma activity. In the fourth stage, oil and gas charged into the reservoirs, with evidence of asphalt filling. Because the first stage of oil and gas filling took place early, the early oil was totally damaged, after multiple structural activities. A previous study identified at least three stages of fluid filling in Member 4 of the Dengying Formation (Liang, 2014). In this study, four stages of diagenetic fluid charging were suggested. The early crude oil accumulation shows the complicated evolution of this oil reservoir.

According to the four phases of fluid activity discussed previously, combined with the diagenetic and thermal evolution histories of source rock in the study area (Figure 2), the timing of diagenetic fluid activity was determined. In the Tongwan period, there might have been hydrocarbon generation from the early Cambrian source rocks in the study area. During the Tongwan movement, the subaerial emergence caused by the uplift of the Gaoshiti area resulted in the oxidation of the crude oil and the disappearance of the residual asphalt. During the two episodes of the Tongwan movement, many weathering fractures developed and were filled with dolomite precipitated from the fresh water. In the early Caledonian period, hydrocarbon generation began, and the second stage of oil was charged into the fractures. In the Indosinian period, the crude oil cracked and the fractures were filled with residual asphalt, dolomite, and quartz. The second phase of asphalt filled the fractures. From the Yanshan to the Himalayan stages, the oil and gas original reservoir adjusted and unfilled open fractures developed.

### 5.2 Identification of subaerial emergence under multi-stage tectonic movement

Under the influence of the Tongwan movement, Member 4 of the Dengying Formation developed many sets of cavity layers and multiple stages of karstification.

#### 5.2.1 Evidence of unconformity

Episode II of the Tongwan movement resulted in the unconformity contact relationship between Member 4 of the Dengying Formation and the upper Maidiping Formation (Figure 8A). Episode III of the Tongwan movement resulted in the unconformity contact between the Cambrian Qiongzhusi and

Fillings	Tungwan period	Caledonian period	Hercynian period	Indosinian period	Yanshanian period	Himalayan period
Stratigraphic state	Shallow burial -Uplift	Middle burial	Uplift	Middle burial	Deep burial	Deep burial
Palaeogeotherm	<60°C	60-120°C	80-120°C	60-160°C	160-220°C	160-220°C
Dolomite	●			●		
Asphalt		●		●		
Calcite				●		
Quartz	●			●		
Saddle dolomite					●	
Fluorite					●	
Barite					●	
Anhydrite					●	
Pyrite					●	
Galena					●	
Sphalerite					●	
Gas				●		●

**FIGURE 6**  
Diagenetic paragenesis of the dolostones from Member 4 of the Dengying Formation, Gaoshiti area, Sichuan Basin.

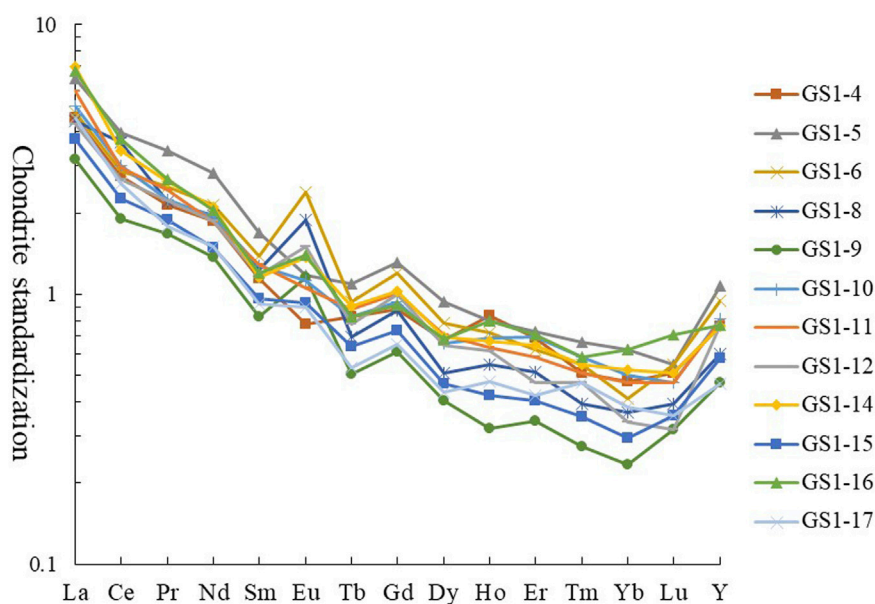
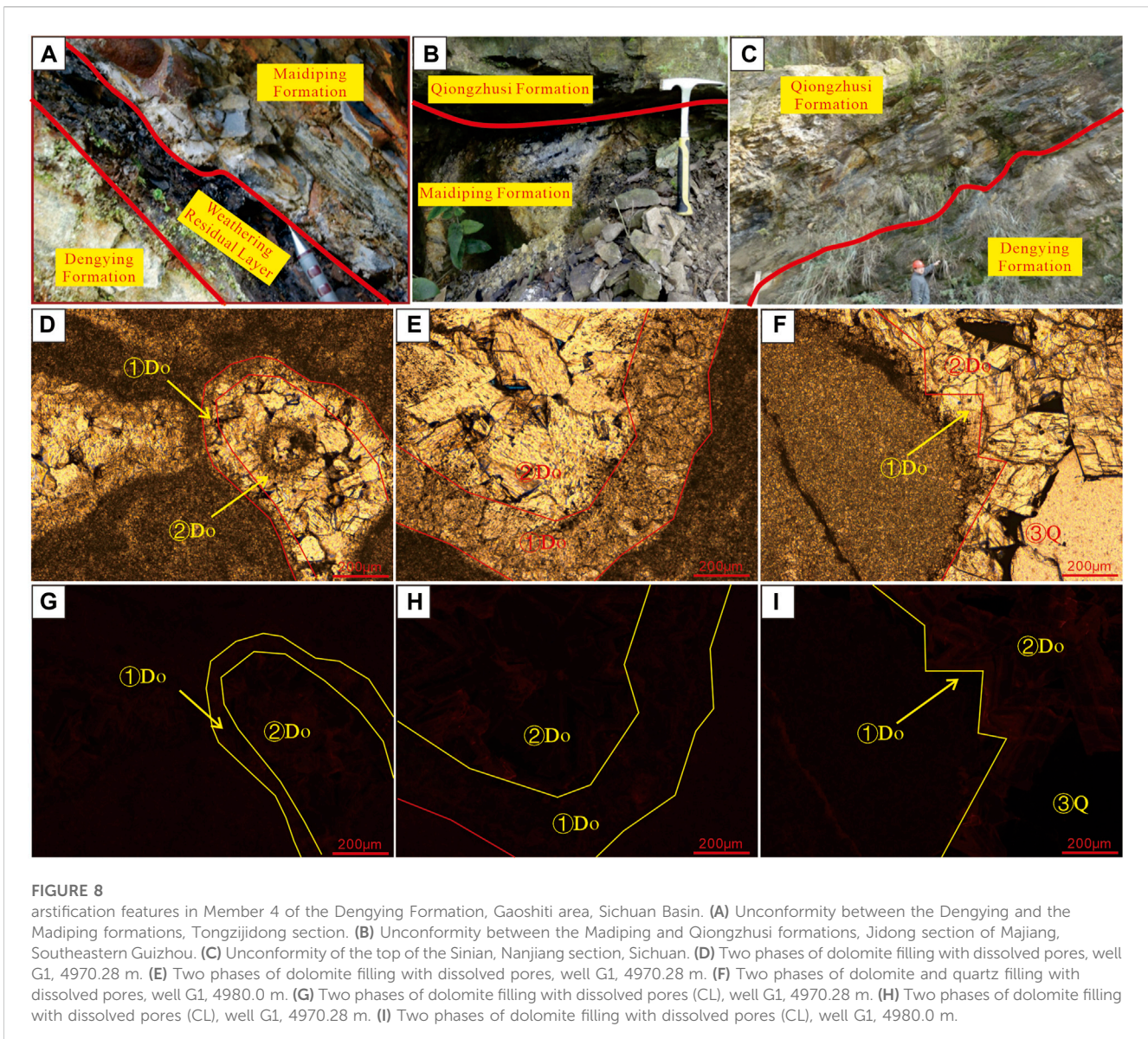


**FIGURE 7**  
REE distribution pattern of dolostones from Member 4 of the Dengying formation, well GS1, Gaoshiti area, Sichuan Basin.

Maidiping Formations (Figure 8B). In some areas, the Maidiping Formation was completely eroded, resulting in direct contact between Member 4 and the lower Cambrian Qiongzhusi

Formation (Figure 8C). Luo et al. (2018) analyzed the age of the limestone strata at the top of Member 4 of the Dengying Formation in the Moxi area (northern Gaoshiti area), suggesting an overlap



between Tongwan Movements II and III. The Gaoshiti area adjacent to the Moxi area also likely underwent two stages of the Tongwan movement.

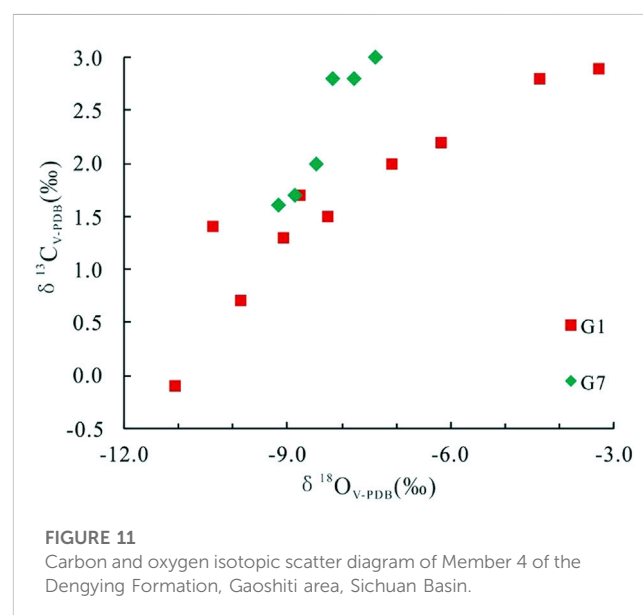
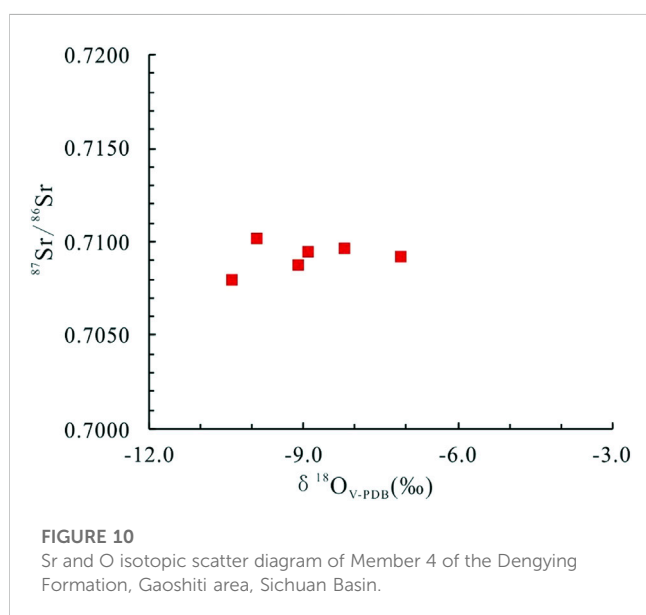
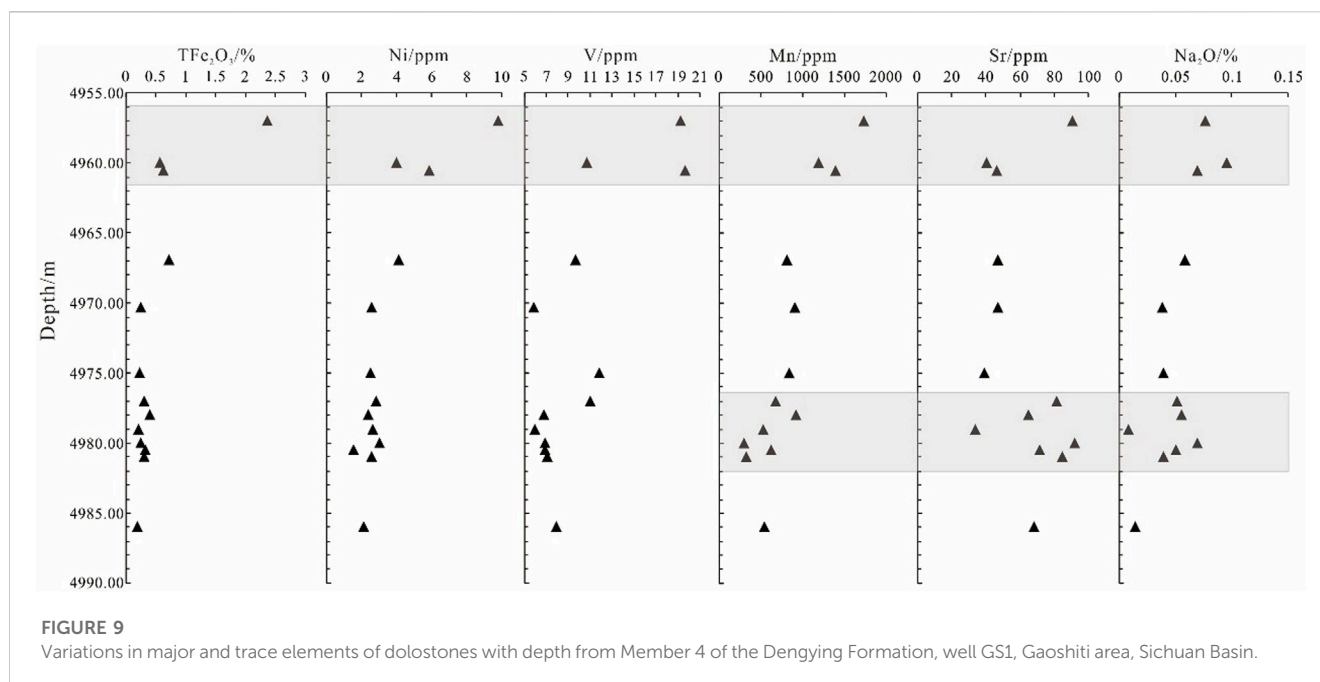
### 5.2.2 Evidence of fillings

In the study area, two stages of the Tongwan movement likely led to two subaerial emergence events. Some dolomite originating from fresh water and quartz often developed in karst cavities. A previous study reported that dolomite filling caused by meteoric water is common in the Tongwan period. The cathodoluminescence (CL) results seemed to show two distinctive CL colors for dolomite (Figures 8D–F). Among them, the CL color of the first phase of dolomite is generally dark brown or dark brown red (Figures 8G–I), while the second phase of dolomite has dark brown-red or dark red CL color (Figures 8H, I). The color of dolomite in these two periods was obviously brighter than that of matrix dolomite, and darker

than that of dolomite formed by hydrothermal fluid during burial diagenesis. Meanwhile, the contemporaneous dolomites are generally fibrous rims, and the crystalline particles of hydrothermal dolomite are coarse in the burial period, while the two phases of meteoric water dolomites formed in the Tongwan movement are mostly fine to medium crystals. It indicates that the two phases of dolomite neither formed in the contemporaneous period, nor in the burial period, but both were products of epidiagenesis. This proves the existence of the two phases of epigenetic karstification in the study area.

### 5.2.3 Evidence of major and trace elements

The profiles of element concentration or element ratios with depth (Figure 9) show that the Fe, Mn, V, Ni, and Sr contents are highest at the top of Member 4. This indicates that the sea level decreases at the top of Member 4 and the oxidizability increases, caused by the Tongwan movement. However, the concentrations of

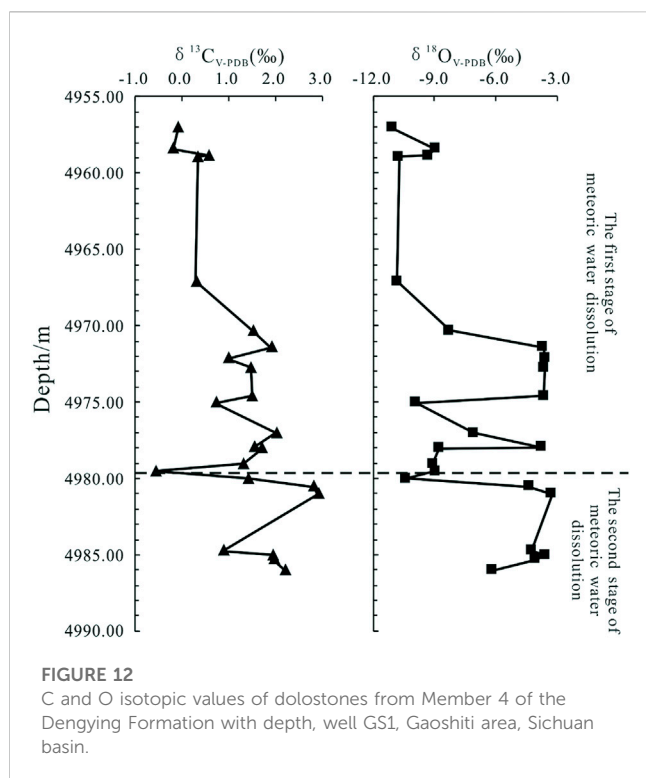


these elements increase again near 4980 m in well GS1 (Figure 9). There may be another stage of subaerial emergence near this depth. Therefore, two stages of karstification likely also developed in the D4 member in the study area.

#### 5.2.4 Evidence of C, O, and Sr isotopes

The  $^{87}\text{Sr}/^{86}\text{Sr}$  ratios of dolomites in the study area were slightly higher than those of contemporaneous seawater. It is generally believed that the increase in radioactive strontium was related to the interaction between meteoric water or hydrothermal fluid and rocks (Nielsen, et al., 1994; Cander, 1995). From the scatter diagram of the Sr and O isotopes,  $^{87}\text{Sr}/^{86}\text{Sr}$  is mainly distributed near 0.7100 (Figure 10). At the same

time,  $\delta^{13}\text{C}$  and  $\delta^{18}\text{O}$  show the characteristics of synchronous negative excursion with  $^{87}\text{Sr}/^{86}\text{Sr}$  in the study area (Figure 11), indicating that the radioactive strontium in microbial rocks of Member 4 in the study area mainly came from meteoric water from the land. Regarding the vertical change of carbon and oxygen isotopes with depth,  $\delta^{13}\text{C}$  and  $\delta^{18}\text{O}$  are obviously divided into two parts at a depth of 4980 m (Figure 12). The two negative excursions of C and O isotopes indicate two periods of meteoric water alteration in the study area. Combined with the two stages of tectonic movement in the study area, the vertical variation of carbon and oxygen isotope characteristics and the change trends of elements were consistent, indicating the existence of two stages of epidiagenesis karstification.



## 5.3 Influences of multi-stage fluid activity and multi-stage karstification on the reservoirs

### 5.3.1 Influences of multi-stage fluid activity on reservoirs

There were four phases of fluid activity in the Gaoshiti area during the burial process. Two phases of oil and gas charging had relatively little impact on the reservoir quality of Member 4 in the study area. The second phase of brine and the third phase of acidic or hydrothermal fluids were accompanied by dissolution and filling. The observation of the pores and fracture types showed that the void spaces mainly consist of dissolved pores, dissolved cavities, and dissolved fractures. In contrast, there are few pores or fractures without the influence of dissolution. This indicates that the reservoir quality in the study area was closely related to the dissolution and has little correlation with the primary sedimentary structure.

The stage of fluid activity occurring in the subaerial exposure in the Tongwan period influenced the reservoir quality. The diagenetic fluid was mainly brine water mixed with meteoric water, with  $\delta^{18}\text{O}$  values ranging from  $-11.1\%$  to  $-3.3\%$  (Figure 11). Meanwhile, on the vertical variation of elements in well GS1 (Figure 9), the seawater shallowing upward and enhanced oxidizability indicated that the D4 member in the study area had the effect of meteoric water. Karstification resulted in the intensive dissolution, and the formation of many non-fabric selective dissolution fractures and cavities (Figures 13A, B). Occasionally, sandstone sedimentation in the underground river can be observed (Figure 13C). With the dissolution, the formation of karst breccia resulted from cavity collapse (Figure 13D). This suggested that karstification was the

key factor for the development of reservoir quality in the Gaoshiti area.

In the third stage, acidic or hydrothermal fluid charging was often accompanied by siliceous filling. The fluid activity in this period generally occurred in the deep burial period, which might be accompanied by dissolution in the burial period (Zhang, 2013; Liang, 2014). In terms of the distribution of fillings on the core, it could be speculated that the acidic or hydrothermal fluid migrated vertically along fractures, and then horizontally along the bedding plane (Figure 13E). Although the horizontal migration of the burial fluid along the bedding plane could result in dissolution in the burial period, a large number of quartz fillings destroyed the new reservoir space (Figure 13F). Under this diagenetic fluid migration model, the dissolution occurred at the bottom and filling developed at the top, resulting in a redistribution of the original pore distribution. Based on the identification of thin sections on the top of the D4 member in wells GS7 and GS18, significant siliceous filling led to a reduction of porosity compared with the dissolution, with minor saddle dolomite filling. It is suggested that the burial dissolution was relatively weak in the study area and the burial diagenesis was characterized by filling.

### 5.3.2 Multi-stage karstification controls on the reservoir

During the subaerial emergence in the Tongwan period, karstification in different paleogeomorphies could alter the primary pore system to produce different extents of dissolution and fillings. Wells GS1 and GS7 are both located on the paleokarst slope (Hao et al., 2017; Jin et al., 2017) and are subject to intensive karstification; thus, widespread dissolved cavities and pores developed. In the depositional period, the tidal flat and lagoon on the restricted platform that developed in GS18 well led to a reservoir with relatively few primary pores compared with the microbial reefs and mounds on the platform margin. However, the upper part of the D4 member in well GS18 affected by the karstification formed many dissolution pores. Therefore, the primary sedimentary structure was almost altered by the karstification, with little influence on the reservoir quality.

In response to the Tongwan movement II and III episodes, the microbialite dolostones of the D4 member were totally altered by karstification, forming two vertical sets of high-quality reservoir zones. The two sets of high-quality karst reservoir zones on the lithological section were identified in the study area. The physical properties, thickness of the valid reservoir, and thickness ratios of the reservoir to the strata of two sets of high-quality reservoir zones were compared statistically (Table 5). The findings suggested that the upper high-quality reservoir zone was formed in episodes II and III of the Tongwan movement, which overlapped the two stages of karstification. The physical properties of the upper reservoir zone are relatively better than those of the lower zone, with an average porosity of 2.78%. The average cumulative thickness of the valid reservoir in the upper reservoir zone is almost 47 m, and the thickness ratio of the reservoir to the strata is close to 15%. Meanwhile, the high-quality reservoir zone in the upper part is mostly distributed within 100 m away from the top of the Sinian. The high-quality reservoir zone in the lower part is relatively far away from the top



**FIGURE 13** Features of fillings and dissolution from Member 4 of the Dengying Formation, Gaoshiti area, Sichuan Basin. (A) Dissolution cavity, well G1, 4967.46–4967.51 m. (B) Unfilled cavity, well G7, 5329.98–5325.16 m. (C) Sandstone filling of the cavity, well G7, 5322.82–5322.93 m. (D) Stylolite, well G7, 5333.92–5334.01 m. (E) Distribution of fracture fillings along the bedding surface, well G7, 5338.51–5338.58 m. (F) Siliceous filling of the spaces among algal laminae, well G2, 5011.39 m.

**TABLE 5** Statistical analyses of the quality and thickness of the reservoirs from Member 4 of the Dengying Formation, Gaoshiti area, Sichuan Basin.

High-quality reservoir zone	Porosity (%)			Permeability (mD)			Thickness ratio of the reservoir to the strata (%)	Distance from the bottom of the reservoir to the top of the Sinian (m)	Accumulated thickness of the reservoir (m)
	Max	Min	Average	Max	Min	Average			
Upper	14.96	0.10	2.78	30.116	0.001	0.453	14.94	113.00	47.00
Lower	9.40	0.15	1.88	48.636	0.001	0.586	7.58	259.00	18.60

of Sinian (Table 5). The reservoir zone in the upper part, which was affected by two rounds of karstification, is of higher quality than that in the lower part, which was only affected by episode II of the Tongwan movement. Therefore, this suggested that episode III of the Tongwan movement after the depositional period of the Madiping Formation had a more important effect on the microbialite reservoir of the D4 member in the Gaoshiti area.

### 6 Conclusion

- (1) Neoproterozoic marine microbialites in this study area have three lithofacies; e.g., thrombolite, stromatolite, and laminate. Thrombolites are more widely distributed than stromatolites in microbial mounds on the margin of intra-shelf depression in Sichuan Basin.
- (2) At least four successive stages of diagenetic fluid charging were observed in the microbialites from Member 4 of the Dengying

- Formation: the first stage was crude oil charging, the second stage was dolomite precipitation, the third stage was quartz precipitation, and the fourth stage was crude oil charging.
- (3) The microbial dolostones in the study area in Member 4 of the Dengying Formation experienced two rounds of karstification, with evidence from the two unconformities, two phases of meteoric water dolomite, two negative excursion events of C and O isotopes, and two cycles of Mn, V, Na, Sr concentration.
- (4) The physical properties of the upper reservoir zone of Member 4 of the Dengying Formation were better than those of the lower reservoir zone. The upper reservoir zone was affected by two rounds of karstification of Tongwan Movement II and III episodes.
- (5) The quality of the microbialite reservoir was improved by strong dissolution during subaerial exposure which increased the secondary porosity. The primary porosity was poorly preserved because it was partly destroyed by the precipitation of quartz cements during late diagenesis.

## Data availability statement

The original contributions presented in the study are included in the article/Supplementary Material; further inquiries can be directed to the corresponding author.

## Author contributions

SD: writing—original draft preparation and editing. MF: conceptualization and methodology. RS: funding acquisition and supervision. HG: validation and visualization. QS: project administration. All authors contributed to the article and approved the submitted version.

## Acknowledgments

The authors thank PetroChina Southwest oil and Gasfield Company for providing rock samples. They appreciate the collaboration with and enthusiastic support from our colleagues Li Tao and Geng Chao from Shunan Gas Production Plant. They

## References

- Amthor, J. E. (2013). "Ara group reservoirs of the South Oman salt basin: Isolated microbial-dominated carbonate platforms in a saline giant," in *Microbial carbonates in space and time: Implications for global exploration and production*. Editors B. Vining, K. Gibbons, W. Morgan, D. Bosence, D. Le Heron, E. Le Ber, et al. (Programme and Abstract), 14–15.
- Bahniuk, A. M., Anjos, S., Franca, A. B., Matsuda, N., Eiler, J., McKenzie, J. A., et al. (2015). Development of microbial carbonates in the Lower Cretaceous Codo Formation (northeast Brazil): Implications for interpretation of microbialite facies associations and palaeoenvironmental conditions. *Sedimentology* 62, 155–181. doi:10.1111/sed.12144
- Bengtson, S., and Zhao, Y. (1992). Predatorial borings in Late Precambrian mineralized exoskeletons. *Science* 257, 367–369. doi:10.1126/science.257.5068.367
- Bosence, D. W. J., Gibbons, K. A., Le Heron, D. P., et al. (2015). *S in space and time: Introduction*, 418. London: Geological Society, London, Special Publications, 1–15.
- Burne, R. V., and Moore, I. S. (1987). Microbialites: Organosedimentary deposits of benthic microbial communities. *Palaios* 2, 241–254. doi:10.2307/3514674
- Cander, H. (1995). "Interplay of water-rock interaction efficiency, unconformities, and fluid flow in a carbonate aquifer: Floridan aquifer system," in *Unconformities and porosity in carbonate strata*. Editors D. A. Budd, A. H. Saller, and P. M. Harris (Tulsa, Oklahoma: American Association of Petroleum Geologists), 103–124. Memoir no. 63.
- Catto, B., Jahnert, R. J., Warren, L. V., Varejao, F. G., and Assine, M. L. (2016). The microbial nature of laminated limestones: Lessons from the upper aptian, araripe basin, Brazil. *Sediment. Geol.* 341, 304–315. doi:10.1016/j.sedgeo.2016.05.007
- Chafetz, H. S. (2013). Porosity in bacterially induced carbonates: Focus on micropores. *AAPG Bull.* 97 (11), 2103–2111. doi:10.1306/04231312173
- Chen, J. T., and Lee, J. H. (2014). Current progress on the geological record of microbialites and microbial carbonates. *Acta Geol. Sin. Engl. Ed.* 88 (1), 260–275. doi:10.1111/1755-6724.12196
- Chen, Zongqing (2010). Gas exploration in sinian Dengying Formation, Sichuan Basin. *China Pet. Explor.* 15 (4), 1–14.
- Davies, G. R., and Smith, L. B., Jr (2006). Structurally controlled hydrothermal dolomitereservoir facies: An overview. *AAPG Bull.* 90, 1641–1690. doi:10.1306/05220605164
- Dupraz, C. D., Visscher, P. T., Baumgartner, L. K., and Reid, R. P. (2004). Microbe-mineral interactions: Early carbonate precipitation in a hypersaline lake (Eleuthera island, Bahamas). *Sedimentology* 51, 745–765. doi:10.1111/j.1365-3091.2004.00649.x
- Fan, C. H., Xie, H. B., Li, H., Zhao, S., Shi, X., Liu, J., et al. (2022). *Complicated Fault characterization and its influence on shale gas preservation in the southern margin of the Sichuan Basin, China*, Cambridge, MA: Harvard University, 8035106. doi:10.2113/2022/8035106
- Frank, J. R., Carpener, A. B., and Oglesby, T. W. (1982). Cathodo-luminescence and composition of calcite cement in the Taum Sauk limestone (upper Cambrian), southeast Missouri. *J. Sediment. Res.* 52, 631–638. doi:10.1306/212F7FB8-2B24-11D7-8648000102C1865D
- Gale, J. F. W., and Gomez, L. A. (2007). Late opening-mode fractures in karst-brecciated dolostones of the Lower Ordovician Ellenburger Group, west Texas: Recognition, characterization, and implications for fluid flow. *AAPG Bull.* 91 (7), 1005–1023. doi:10.1306/03130706066
- Grotzinger, J. P., Watters, W. A., and Knoll, A. H. (2000). Calcified metazoans in thrombolite-stromatolite reefs of the terminal Proterozoic Nama Group, Namibia. *Paleobiology* 26, 334–359. doi:10.1666/0094-8373(2000)026<0334:cmitrs>2.0.co;2
- Gu, Yifan, Wang, Zhanlei, Yang, Changcheng, Luo, M., Jiang, Y., Luo, X., et al. (2023). Effects of diagenesis on quality of denying formation deep dolomite reservoir, Central Sichuan Basin, China: Insights from petrology, geochemistry and *in situ* U-Pb dating. *Front. Earth Sci.* 10, 1041164. doi:10.3389/feart.2022.1041164
- Hao, Y., Yang, X., Wang, Y. F., et al. (2017). Study on the surface karstification of Dengying Formation in Sichuan Basin. *Sediment. Geol. Tethys Geol.* 37 (01), 48–54.
- Hartnady, C. J. H. (1986). Was North America (laurentia) part of southwestern gondwanaland during the late proterozoic era. *S Afr J Earth Sci.* 82, 251–254.
- Huang, Jiqing, Ren, Jishun, Jiang, Chunfa, et al. (1974). New understanding of some characteristics of geotectonics in China. *Acta Geol. Sin.* 53 (1), 36–52.
- Jin, Mindong, Tan, Xiucheng, Tong, Mingsheng, Zeng, W., Liu, H., Zhong, B., et al. (2017). Karst paleogeomorphology of the fourth member of sinian Dengying Formation in gaoshiti-moxi area, Sichuan Basin, SW China: Restoration and geological significance. *Petroleum Explor. Dev.* 44 (1), 58–68. doi:10.1016/s1876-3804(17)30008-3
- Liang, J. J. (2014). *Study on the hydrocarbon accumulation of the sinian-lower paleozoic in the sichuan-central Sichuan Basin in the Sichuan Basin*. Chengdu, China: Chengdu University of Technology.
- Liang, X., Liu, S., and Wang, S. (2019). Analysis of the oldest carbonate gas reservoir in China—new geological significance of the denying gas reservoir in the weiyun structure, Sichuan Basin. *J. Earth Sci.* 2, 348–366. doi:10.1007/s12583-017-0962-y
- Liao, W., He, X. Q., and Luo, Q. H. (1999). The evolution sequence of Sichuan prototype basin and the development law of composite basin. *Nat. Gas Explor. Dev.* 4, 6–13.
- Liu, Quanyou, Zhu, Dongya, Jin, Zhijun, Liu, C., Zhang, D., and He, Z. (2016). Coupled alteration of hydrothermal fluids and thermal sulfate reduction (TSR) in ancient dolomite reservoirs – an example from Sinian Dengying Formation in Sichuan Basin, southern China. *Precambrian Res.* 285, 39–57. doi:10.1016/j.precamres.2016.09.006

thank the State Key Laboratory of Oil and Gas Reservoir Geology and Exploitation in China for the measurement.

## Conflict of interest

Author QS was employed by the company PetroChina Southwest Oil and Gasfield Company.

The remaining authors declare that the research was conducted in the absence of any commercial or financial relationships that could be construed as a potential conflict of interest.

## Publisher's note

All claims expressed in this article are solely those of the authors and do not necessarily represent those of their affiliated organizations, or those of the publisher, the editors, and the reviewers. Any product that may be evaluated in this article, or claim that may be made by its manufacturer, is not guaranteed or endorsed by the publisher.

- Luo, Beiwei, Guoqi, Wei, Yang, Wei, et al. (2013). Reconstruction of the late Sinian paleo-ocean environment in Sichuan basin and its geological significance. *Chin. Geol.* 40 (4), 1099–1111.
- Luo, Bing, Yang, Yueming, Luo, Wenjun, et al. (2015). Controlling factors and distribution of reservoir development in Dengying Formation of paleouplift in central Sichuan Basin. *Acta Pet. Sin.* 36 (4), 416–426. doi:10.7623/syxb201504003
- Mancini, E. A., Morgan, W. A., Harris, P. M., and Parcell, W. C. (2013). Introduction: AAPG hedberg research conference on microbial carbonate reservoir characterization—conference summary and selected papers. *AAPG Bull.* 97 (11), 1835–1847. doi:10.1306/intro070913
- Mo, Y. (2017). *Study on characteristics of carbonate reservoirs in the fourth member of the sinian Dengying Formation in gaoshiti-moxi*. Chengdu, China: Chengdu University of Technology.
- Narbonne, G. M. (2005). *The ediacarabiota: Neoproterozoic origin of animals and their ecosystems*. Palo Alto: Annual Review of Earth and Planetary Sciences, 421–442.
- Nielsen, R. L., Forsythe, L. M., Gallahan, W. E., and Fisk, M. R. (1994). Major- and trace-element magnetite-melt equilibria. *Chem. Geol.* 117, 167–191. doi:10.1016/0009-2541(94)90127-9
- Piper, J. D. A. (2000). The neoproterozoic supercontinent: Rodinia or palaeopangea? *Earth Planet. Sci. Lett.* 176, 131–146. doi:10.1016/s0012-821x(99)00314-3
- Riding, R. (2000). Microbial carbonates: The geological record of calcified bacterial algal mats and biofilms. *Sedimentology* 47 (Suppl. 1), 179–214. doi:10.1046/j.1365-3091.2000.00003.x
- Roehl, P. O., and Choquette, P. W. (1985). *Carbonate Petroleum. Reservoirs*. Berlin: Springer.
- Shapiro, R. S. (2000). A comment on the systematic confusion of thrombolites. *Palaios* 15, 166–169. doi:10.1669/0883-1351(2000)015<0166:acotsc>2.0.co;2
- Tang, H., Kershaw, S., Liu, H., Tan, X., Li, F., Hu, G., et al. (2017). Permian-Triassic boundary microbialites (PTBMs) in south-west China: Implications for paleoenvironment reconstruction. *Facies* 63 (2), 2. doi:10.1007/s10347-016-0482-8
- Terra, G. J. S., Spadini, A. R., Franca, A. B., et al. (2010). *Carbonate rock classification applied to Brazilian sedimentary basins*, 18. Rio de Janeiro: Boletim de Geociencias da Petrobras, 9–29.
- Tong, C. G. (1992). *Tectonic evolution and hydrocarbon accumulation in the Sichuan Basin*. Beijing: Geological Publishing House.
- Wang, Zecheng, Jiang, Hua, Wang, Tongshan, Lu, W., Gu, Z., Xu, A., et al. (2014). Paleogeomorphology formed during Tongwan tectonization in Sichuan Basin and its significance for hydrocarbon accumulation. *Pet. Explor. Dev.* 41 (3), 338–345. doi:10.1016/s1876-3804(14)60038-0
- Wei, Guoqi, Yang, Wei, Du, Jinghu, et al. (2015). Geological characteristics of the sinian-early cambrian intracratonic rift, Sichuan Basin. *Nat. Gas. Ind.* 35 (1), 24–35. doi:10.3787/j.issn.1000-0976.2015.01.003
- Woo, J., and Chough, S. K. (2010). Growth patterns of the cambrian microbialite: Phototropism and speciation of epiphyton. *Sediment. Geol.* 229, 1–8. doi:10.1016/j.sedgeo.2010.05.006
- Xia, Qinyu, Haijun, Yan, Xu, Wei, Zhang, L., Li, Q., Luo, W., et al. (2022). Paleo-karst zone and its control on reservoirs in the fourth member of the Sinian Dengying formation in the Moxi area, central Sichuan Basin. *Carbonates Evaporites* 37, 48. doi:10.1007/s13146-022-00788-z
- Xu, Zhehang, Lan, Caijun, Zhang, Benjian, Hao, F., Lu, C., Tian, X., et al. (2022). Impact of diagenesis on the microbial reservoirs of the terminal ediacaran Dengying Formation from the central to northern Sichuan Basin, SW China. *Mar. Petroleum Geol.* 146, 105924. doi:10.1016/j.marpetgeo.2022.105924
- Yan, Ruijing, Xu, Guosheng, Xu, Fanghao, Song, J., Yuan, H., Luo, X., et al. (2022). The multistage dissolution characteristics and their influence on mound-shoal complex reservoirs from the Sinian Dengying Formation, southeastern Sichuan Basin, China. *Mar. Petroleum Geol.* 139, 105596. doi:10.1016/j.marpetgeo.2022.105596
- Yang, Jiedong, Sun, Weiguo, Wang, Zongzhe, Yaosong, X., and Xiancong, T. (1999). Variations in Sr and C isotopes and Ce anomalies in successions from China: Evidence for the oxygenation of neoproterozoic seawater? *Precambrian Res.* 93, 215–233. doi:10.1016/s0301-9268(98)00092-8
- Yang, W., Wei, G. Q., Zhao, R. R., et al. (2014a). Characteristics and distribution of karst reservoirs in the sinian Dengying Formation of the Sichuan Basin. *Nat. Gas. Ind.* 34 (03), 55–60. doi:10.3787/j.issn.1000-0976.2014.03.009
- Yang, Yu, Huang, Xianping, Zhang, Jian, et al. (2014b). Feature and geologic significances of the top sinian karst landform before the cambriandeposition in the Sichuan Basin. *Nat. Gas. Ind.* 34 (3), 38–43. doi:10.3787/j.issn.1000-0976.2014.03.006
- Yang, Yu, Huang, Xianping, Zhang, Jian, et al. (2014c). Karst geomorphic characteristics and geological significance of Sinian top boundary before Cambrian sedimentation in Sichuan Basin. *Nat. Gas. Ind.* 34 (3), 38–43. doi:10.3787/j.issn.1000-0976.2014.03.006
- Zhang, S. (2013). *Study on the formation mechanism of high-quality reservoirs in the Dengying Formation of the high-stone ladder in central Sichuan*. Chengdu, China: Chengdu University of Technology.
- Zhang, T. G., Chu, X. L., Zhang, Q. B., et al. (2004). The sulfur and carbon isotopic records in carbonates of the Dengying Formation in the Yangtze Platform, China. *Acta Petrol. Sin.* 20, 717–724. doi:10.2116/analsci.20.717
- Zhu, Dongya, Jin, Zhijun, Zhang, Rongqiang, et al. (2014). Characteristics and developing mechanism of Sinian Dengying Formation dolomite reservoir with multi-stage karst. *Earth Sci. Front.* 21 (6). doi:10.13745/j.esf.2014.06.032